



Oxidative access to flexible $\{\text{Pt}_2(\mu\text{-SAr})_2\}$ square motifs from platinum thiolato complexes with chelating diphosphine

Su-Kyung Lee^a, Olivier Jeannin^b, Marc Fourmigué^b, Wooyoung Suh^a, Dong-Youn Noh^{a,*}

^a Department of Chemistry, Seoul Women's University, Seoul 139-774, South Korea

^b Institut des Sciences Chimiques de Rennes, Université de Rennes 1, UMR CNRS 6226, Rennes 35042, France

ARTICLE INFO

Article history:

Received 11 May 2012

Received in revised form

29 June 2012

Accepted 3 July 2012

Keywords:

Heteroleptic $\text{P}_2\text{Pt}(\text{II})\text{S}_2$ complex

Aryl thiolate

$\{\text{Pt}_2(\mu\text{-SR})_2\}$ square motif

Oxidative dimerization

X-ray crystal structure

ABSTRACT

Platinum(II) aryl thiolate complexes formulated as $(\mathbf{P2})\text{Pt}(\text{SAr})_2$ are prepared from the chelating bis(diphenylphosphino)dimethyltetrathiafulvalene ($\mathbf{P2}$), with aryl thiolate ligands (SAr), such as benzene-thiolate (BT) and 3,5-dimethylbenzenethiolate (DMBT). The structurally characterized neutral $(\mathbf{P2})\text{Pt}(\text{SAr})_2$ complexes afford, upon oxidation with TCNQF_4 , dicationic bimetallic Pt(II) complexes formulated as $[(\mathbf{P2})\text{Pt}(\mu\text{-SAr})_2\text{Pt}(\mathbf{P2})]^{2+}$, characterized by a flexible $\{\text{Pt}_2(\mu\text{-SAr})_2\}$ square motif. The magnetic properties of the TCNQF_4^- salts of these bimetallic Pt(II) complexes are determined from susceptibility measurements and a tentative rationale for the formation of such $\{\text{Pt}_2(\mu\text{-SAr})_2\}$ square complexes are provided, based on an original oxidative dimerization process.

© 2012 Elsevier B.V. All rights reserved.

1. Introduction

Square-planar palladium(II) and platinum(II) complexes have been intensively investigated for their structural diversity [1,2], anticancer activity [3], catalytic effect [4] and photochemical properties [5], as well as their capacity to sustain reversible oxidation to the radical state, toward the formation of conducting materials [6]. Mononuclear systems with $\{\text{P}_2\text{PtS}_2\}$ coordination motifs are especially attractive in this respect, specifically those with chelating dithiolate ligands or with redox active diphosphines such as 1,1'-bis(diphenylphosphino)ferrocene (dppf) [7,8] or 3,4-dimethyl-3',4'-bis(diphenylphosphino) tetrathiafulvalene (hereafter, abbreviated as $\mathbf{P2}$) [9–11]. Indeed, the 16-electron (diphosphine)Pt(dithiolene) complexes, for example, (dppe)Pt(dmit) [12] (dmit: 2-thio-1,3-dithiole-4,5-dithiolato; dppe: 1,2-bis(diphenylphosphino)ethane) or (dppe)Pt(dddt) [10] (dddt: 4,5-dihydro-1,4-dithiine-2,3-dithiolato) (Scheme 1), have shown reversible oxidation as the cation radical state. This is attributed to the non-innocent character of the dithiolene ligands.

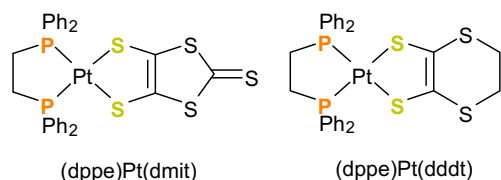
Redox activity can also be observed on diphosphine ligand itself, for example in ferrocene-based complexes $(\text{dppf})\text{Pt}(\text{SR})_2$ ($\text{R} = \text{Ph}$ [8], ^nPr [8], C_6F_5 [13], $p\text{-C}_6\text{HF}_4$ [7a]). However, in these complexes, irreversible redox processes associated to the thiolate ligands were observed before ferrocene oxidation. A combination of both redox active dppf and dithiolene ligands was also reported, as in $(\text{dppf})\text{Pt}(\text{bdt})$ [14] (bdt: 1,2-benzenedithiolate) or $(\text{dppf})\text{Pt}(\text{dmit})$ [7c] (Scheme 2). In these complexes, two reversible oxidation waves were observed, which were attributed to the oxidation of the ferrocene core and the Pt(dithiolene) metallacycle, respectively.

Similarly, in tetrathiafulvalenyl-based $(\mathbf{P2})\text{Pt}(\text{dithiolene})$ complexes such as $(\mathbf{P2})\text{Pt}(\text{dmit})$ or $(\mathbf{P2})\text{Pt}(\text{dddt})$ (Scheme 3) [10,11], up to four oxidation waves were identified, which were attributed to the sequential oxidation of the independent redox moieties, namely the TTF core on the one hand and the Pt(dddt) moiety on the other hand.

In this respect, it is of interest to investigate the corresponding simple bis(monothiolate) derivatives, $(\mathbf{P2})\text{Pt}(\text{SR})_2$, in order to determine their redox behavior and their capacity to form radical species, compared to the corresponding dithiolene analogs. We describe herein the preparation, structural and electronic properties of two $(\mathbf{P2})\text{Pt}(\text{SAr})_2$ complexes with different aryl thiolate (SAr) ligands. Their oxidation with TCNQF_4 led to unexpected dicationic bimetallic $[(\mathbf{P2})\text{Pt}(\mu\text{-SAr})_2\text{Pt}(\mathbf{P2})]^{2+}$ complexes. The structure and magnetic properties of these TCNQF_4^- radical salts are described and a rationale is proposed for the formation of these flexible

* Corresponding author. Tel.: +82 2 970 5656; fax: +82 2 970 5972.

E-mail address: dynoh@swu.ac.kr (D.-Y. Noh).



Scheme 1. (dppe)Pt(dithiolate) complexes.

{Pt₂S₂} motifs, which are currently the subject of renewed interest because of their attractive flexibility and reactivity [15,16].

2. Results and discussion

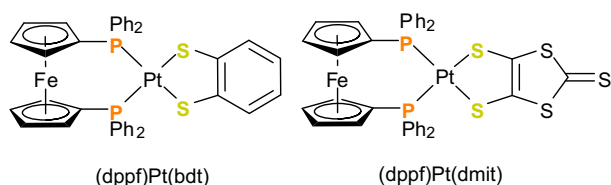
2.1. Syntheses

The thiolate (P2)Pt(SAr)₂ complexes where SAr is benzene-thiolate (BT), or 3,5-dimethylbenzenethiolate (DMBT), were prepared as previously described for dithiolene complexes [10,11], by the metathesis reaction of (P2)PtCl₂ [9g] with the corresponding arylthiols (ArSH) in the presence of NEt₃ (Scheme 4). Purification by column chromatography afforded the products in 60% yield. In order to evaluate the respective role of the TTF core and the bis(-thiolate)Pt moiety in the electrochemical properties of these complexes, (dppe)Pt(BT)₂ [17] and (dppe)Pt(DMBT)₂ [18] were prepared as described above. They were also obtained by another route using lead thiolates [19], potentially a good alternative, since the side-product (PbCl₂) precipitates out from the reaction mixture but reaction yields were disappointing (15%).

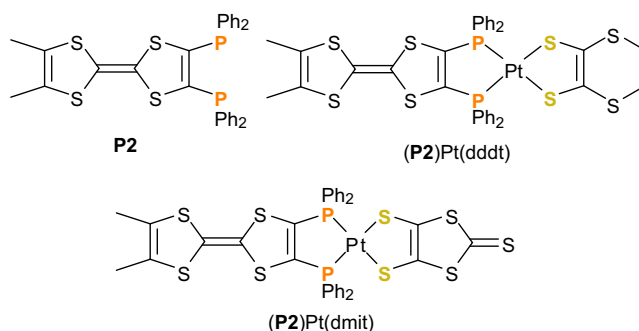
All of the platinum(II) complexes were characterized by spectroscopic methods such as FT-IR, NMR, UV/vis and/or MALDI-TOF MS. Actually, in the mass spectra of the (P2)Pt(SAr)₂ complexes, the intensities for the M⁺ peak are less than 1%, while those for (M⁺ - SAr) are 100%, indicating that the loss of one monothiolate ligand to give a fragment of [(P2)Pt(SAr)]⁺ is favored under such measurement conditions. This result contrasts strongly with those described earlier for (P2)Pt(dithiolene) complexes incorporating a chelating 1,2-dithiolate moiety, where the intensity of the (M⁺ + 1) peak was reported to be 100% [10]. This behavior also indicates that the bis(monothiolate) complexes described herein are less stable than their corresponding dithiolate analogs, which is a consequence of the absence of the chelate effect.

2.2. Electrochemical properties

The cyclic voltammograms of (P2)PtCl₂, (P2)Pt(BT)₂ and (P2)Pt(DMBT)₂ are compared in Fig. 1 and the numerical data are collected in Table 1. While (P2)PtCl₂ exhibits two reversible redox waves upon oxidation, attributed to the redox behavior of TTF core [9g], an additional shoulder is clearly identified at lower potentials in the two aryl thiolate complexes, with an associated anodic shift of the two following reversible waves. This behavior might indicate the existence of a first oxidation process affecting the electron-rich thiolate ligands before TTF oxidation itself. In order to test this



Scheme 2. (dppf)Pt(dithiolate) complexes.



Scheme 3. P2 free ligand and (P2)Pt(dithiolate) complexes.

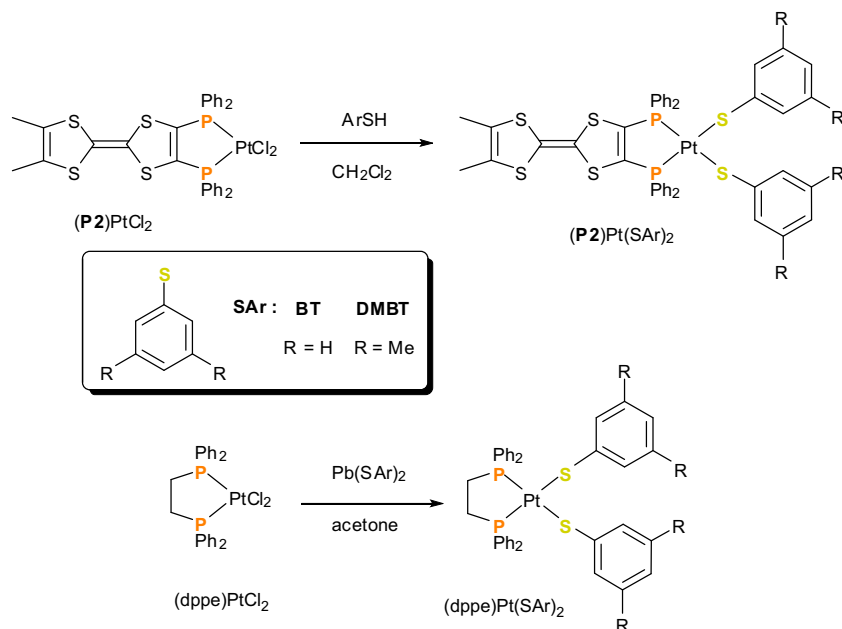
assumption, we also investigated the electrochemical response of the analogous dppe complexes described above, which lack the redox active TTF core. As shown in Fig. 2, the oxidation of (dppe)Pt(BT)₂ clearly shows an irreversible wave at exactly the same potential where the shoulder was found in the oxidation of (P2)Pt(BT)₂. We can tentatively conclude that the first irreversible process is associated with thiolate oxidation, leaving a cationic intermediate [(P2)Pt(BT)]⁺ species. The reversible oxidation processes observed at higher potentials in (P2)Pt(BT)₂ and (P2)Pt(DMBT)₂ (Fig. 1) are thus attributable to the TTF core oxidation, shifted to more anodic potentials than is (P2)PtCl₂ because of the positive charge of the intermediate.

The oxidation of the (P2)Pt(SAr)₂ complexes were also investigated chemically by reacting them with TCNQF₄, a well known electron acceptor whose reduction potential to the TCNQF₄⁻ radical anion (0.53 V vs SCE [20], ≈0.75 V vs Ag/AgCl) approximately matches with the oxidation potential of the (P2)Pt(SAr)₂ complexes [21]. Mixing solution of the two compounds immediately afforded a dark green colored solution from which crystals could be obtained. X-ray crystal structure determinations (see below) showed that the oxidation had indeed affected the electron-rich thiolate ligands, since bimetallic dicationic species formulated as [(P2)Pt(μ-SAr)₂Pt(P2)]²⁺ were identified, which co-crystallized with two TCNQF₄⁻ radical anions.

2.3. Structural properties

Crystal structures could be obtained from X-ray diffraction on single crystals for the two neutral complexes (P2)Pt(BT)₂ and (P2)Pt(DMBT)₂, together with their TCNQF₄ oxidation products. As shown in Fig. 3, the coordination chemistry around the Pt atom in (P2)Pt(BT)₂ and (P2)Pt(DMBT)₂ is close to square planar with dihedral angles between the P₂Pt and S₂Pt mean planes of 8.04(3)° and 6.86(3)° in (P2)Pt(DMBT)₂ and (P2)Pt(BT)₂, respectively. Similarly, the TTF moiety is essentially planar, in contrast with other P2-metal complexes where a stronger folding of the dithiole rings along the S...S hinges has been reported [9]. The bond distances and angles (Table 2) in the Pt coordination sphere are comparable with those described for analogous complexes such as (dppe)Pt(BT)₂ [22], (dppv)Pt(BT)₂ [23], (dppe)Pt(S-C₆F₅)₂, or (dppe)Pt(S-C₆H₄(o-CF₃))₂ [24].

The oxidation of the complexes with TCNQF₄ afforded two salts incorporating the dicationic [(P2)Pt(μ-BT)₂Pt(P2)]²⁺ and [(P2)Pt(μ-DMBT)₂Pt(P2)]²⁺ species (Fig. 4). Since the BT-derivative is located at an inversion center (Fig. 4a), the {Pt₂S₂} square metallacycle is planar as shown in Fig. 5a. On the other hand, it adopts a butterfly shape in the DMBT-derivative (Fig. 5b) with a folding angle between the two PtS₂ planes of 147.24(8)°. This difference between



Scheme 4. Syntheses of $(\mathbf{P2})\text{Pt}(\text{SAr})_2$ and $(\text{dppe})\text{Pt}(\text{SAr})_2$.

these two otherwise similar complexes illustrates the flexibility of these square motifs, as discussed below.

$[(\text{P}-\text{P})\text{Pt}(\mu\text{-SR})_2\text{Pt}(\text{P}-\text{P})]^{2+}$ complexes with a planar $\{\text{Pt}_2\text{S}_2\}$ core usually have an *anti* conformation, R-groups pointing in opposite directions, as in $[(\mathbf{P2})\text{Pt}(\mu\text{-BT})_2\text{Pt}(\mathbf{P2})]^{2+}$ and other such compounds [15]. On the contrary, complexes with a hinged $\{\text{Pt}_2\text{S}_2\}$ core dominantly have a *syn-exo* conformation (R-groups on the same side) [16d,24,25], possibly because the hinged $\{\text{Pt}_2\text{S}_2\}$ core sterically prefers the *syn-exo* conformation rather than the sterically unfavored *anti* conformation. Therefore, to our knowledge, the $[(\mathbf{P2})\text{Pt}(\mu\text{-DMBT})_2\text{Pt}(\mathbf{P2})]^{2+}$ complex with a hinged $\{\text{Pt}_2\text{S}_2\}$ core is the first compound that has an *anti* conformation. This sterically unfavored conformation is allowed in this complex possibly due to the comparatively bulky DMBT bridging and $\mathbf{P2}$ terminal ligands. The intramolecular Pt...Pt distance in the $\{\text{Pt}_2\text{S}_2\}$ core is moderately short (3.607(6) Å) in the BT-derivative and shorter in DMBT-derivative (3.4562(7) Å) where the $\{\text{Pt}_2\text{S}_2\}$ core is hinged along the S...S axis. On the other hand, the intramolecular S...S distances do not vary significantly (3.116(8) Å and 3.082(4) Å, respectively) as

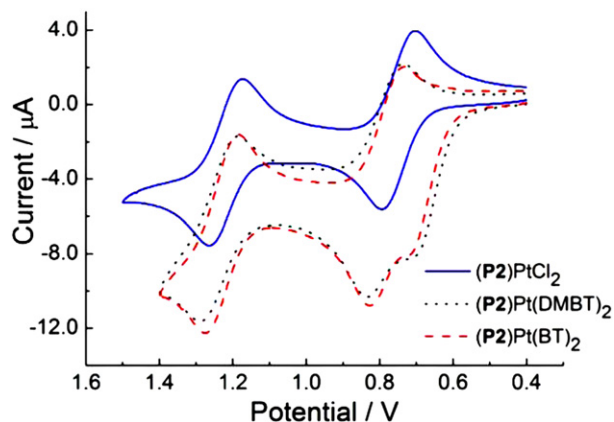


Fig. 1. The cyclic voltammograms of the $(\mathbf{P2})\text{Pt}$ complexes measured in CH_2Cl_2 ($\text{Fc}/\text{Fc}^+ = 0.565$ V vs Ag/AgCl).

the $\{\text{Pt}_2\text{S}_2\}$ core is hinged (Tables 3 and 4). The coordination around the Pt atom is still very close to square-planar, with angles between the PtS_2 and PtP_2 planes of $6.4(5)^\circ$ in the BT-derivative and $6.0(9)^\circ$ and $6.5(9)^\circ$ in the DMBT-one.

The central C=C bond distance is a valuable indicator of the oxidation state of the TTF as it adopts a short length in the reduced form, while the lengthening of this bond accompanies the oxidation of TTF, up to a full single bond character in the TTF^{2+} dication [26]. The C=C bond distances in $(\mathbf{P2})\text{Pt}(\text{DMBT})_2$ and $(\mathbf{P2})\text{Pt}(\text{BT})_2$ amount to 1.351(6) and 1.334(7) Å, respectively. Turning to the dicationic bimetallic species, these C=C bond distances are found at comparable values, 1.343(8) Å in the centrosymmetric BT-derivative and 1.337(16) and 1.351(16) Å in the DMBT-one. The close proximity of these values clearly confirms that the TTF moieties are not oxidized in these dicationic complexes. This becomes more obvious if they are compared with the C=C bond distances of the oxidized TTF moiety of a $\mathbf{P2}$ radical cation, $[(\mathbf{P2})\text{Mo}(\text{CO})_4]_2[\text{Mo}_6\text{O}_{19}]$ (1.388(5) Å) [27]. The dicationic charge in $[(\mathbf{P2})\text{Pt}(\mu\text{-BT})_2\text{Pt}(\mathbf{P2})]^{2+}$ and $[(\mathbf{P2})\text{Pt}(\mu\text{-DMBT})_2\text{Pt}(\mathbf{P2})]^{2+}$ is therefore concentrated on the $\{\text{P}_2\text{PtS}_2\}$ core. Besides, since the redox process involved the TCNQF_4 as an oxidant (toward the thiolate ligand), the latter is now reduced in its radical TCNQF_4^- anion form. This state is unambiguously confirmed by several observations, (1) the averaged distances of C–C (1.422(5) Å) and C=C (1.361(6) Å) bonds in the quinone ring, and those of C–F (1.351(4) Å) and C≡N (1.157(6) Å) bonds in TCNQF_4 , (2) the IR $\nu(\text{C}\equiv\text{N})$ stretching frequency observed at 2192 cm^{-1} compared to that of neutral TCNQF_4 (2226 cm^{-1}), all

Table 1
Cyclic voltammetry data for the $(\mathbf{P2})\text{Pt}$ complexes.^a

Complex	E_{pa}^1	E_{pa}^2	E_{pa}^3	E_{pc}^2	E_{pc}^3	$E_{1/2}^2$ ^b	$E_{1/2}^3$ ^b
$(\mathbf{P2})\text{PtCl}_2$		0.777	1.245	0.691	1.166	0.734	1.206
$(\mathbf{P2})\text{Pt}(\text{DMBT})_2$	0.706	0.833	1.290	0.736	1.181	0.785	1.236
$(\mathbf{P2})\text{Pt}(\text{BT})_2$	0.732	0.827	1.276	0.733	1.184	0.780	1.230

^a 50 mV s^{-1} scan rate; Supporting electrolyte: 0.1 M $n\text{-Bu}_4\text{N}^+\text{PF}_6^-$; Working Electrode: Pt disk; Counter electrode: Pt wire; Ref. electrode: Ag/AgCl ; 1 mM samples in CH_2Cl_2 ; $E_{1/2} = 0.565$ V for Fc^+/Fc .

^b $E_{1/2} = (E_{\text{pa}} + E_{\text{pc}})/2$.

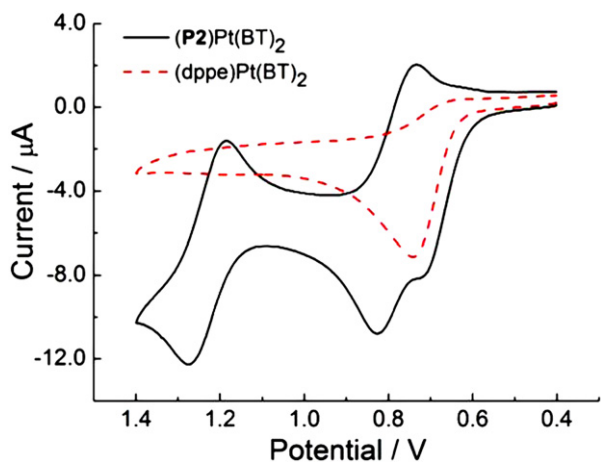


Fig. 2. Comparison of cyclic voltammograms of $(\mathbf{P2})\text{Pt}(\text{BT})_2$ and $(\text{dppe})\text{Pt}(\text{BT})_2$ measured in CH_2Cl_2 ($\text{Fc}/\text{Fc}^+ = 0.565$ V vs Ag/AgCl).

unambiguously correspond to those of the TCNQF_4^- radical anion [28,29].

2.4. Magnetic properties in the solid state

The temperature dependence of the magnetic susceptibility of both TCNQF_4^- salts (Fig. 6) show weak paramagnetism with the susceptibility going through a rounded maximum, around room temperature for the DMBT-salt and above room temperature for the BT-salt. This behavior is characteristic of antiferromagnetic interactions which settle between the TCNQF_4^- radical species.

Actually, the solid state arrangement in the BT-salt (Fig. 7) shows that the TCNQF_4^- moieties are associated two-by-two and sandwiched between the planar TTF moieties in the $\mathbf{P2}$ ligand. A similar organization is also found for the DMBT-salt (Fig. 8), even though the TTF moieties are also facing each other. The overlap interaction between the TCNQF_4^- radical species is shown in Fig. 9. Of particular note is the short intermolecular C...C distances within these dianionic dyads, which are as short as 3.166(10) Å in the BT-salt and 3.05(1) Å in the more distorted DMBT-salt. These very short contacts allow for a strong interaction between the singly occupied TCNQF_4^- LUMOs, leading to the formation of (fully filled) bonding and (empty) antibonding combinations. Accordingly, the

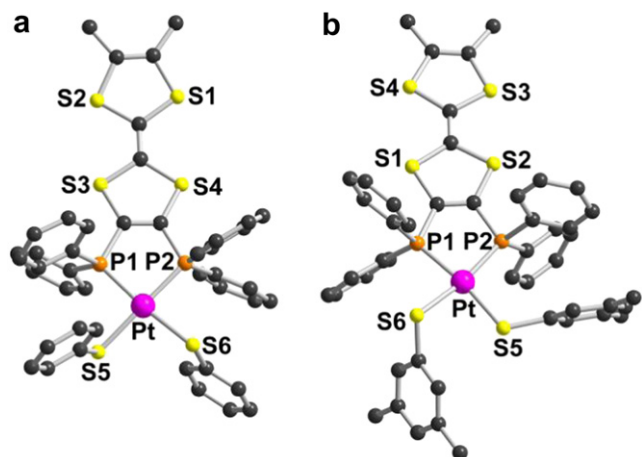


Fig. 3. Molecular structures of (a) $(\mathbf{P2})\text{Pt}(\text{BT})_2$ and (b) $(\mathbf{P2})\text{Pt}(\text{DMBT})_2$.

Table 2
Selected bond distances (Å) and angles ($^\circ$) for $(\mathbf{P2})\text{Pt}(\text{BT})_2$ and $(\mathbf{P2})\text{Pt}(\text{DMBT})_2$.

$(\mathbf{P2})\text{Pt}(\text{BT})_2$		$(\mathbf{P2})\text{Pt}(\text{DMBT})_2$	
Pt–P(1)	2.2362(10)	Pt–P(1)	2.2459(12)
Pt–P(2)	2.2324(10)	Pt–P(2)	2.2429(12)
Pt–S(5)	2.3729(10)	Pt–S(5)	2.3348(12)
Pt–S(6)	2.3787(9)	Pt–S(6)	2.3808(11)
S(5)–C(33)	1.762(4)	S(5)–C(33)	1.780(5)
S(6)–C(39)	1.766(4)	S(6)–C(41)	1.775(5)
P(1)–Pt–P(2)	88.63(4)	P(1)–Pt–P(2)	87.92(4)
P(1)–Pt–S(5)	90.57(4)	P(1)–Pt–S(5)	171.56(4)
P(2)–Pt–S(5)	174.36(3)	P(2)–Pt–S(5)	100.43(4)
P(1)–Pt–S(6)	173.43(3)	P(1)–Pt–S(6)	84.75(4)
P(2)–Pt–S(6)	86.51(3)	P(2)–Pt–S(6)	169.22(4)
S(5)–Pt–S(6)	94.70(4)	S(5)–Pt–S(6)	87.14(4)

temperature dependence of the magnetic susceptibility of both salts was fitted within the singlet-triplet model (Bleaney–Bowers) with

$$\chi = \chi_0 + x\chi_{\text{Curie}} + \left(1 - x\right) \frac{3Ng^2\beta^2}{kT[3 + \exp(-J/kT)]}$$

where χ_0 is a temperature-independent contribution, x the fraction of Curie-type magnetic defaults and J the magnetic coupling interaction, giving $\chi_0(\text{BT}) = 5 \times 10^{-5} \text{ cm}^3 \text{ mol}^{-1}$, $\chi_0(\text{DMBT}) = 8.8 \times 10^{-4} \text{ cm}^3 \text{ mol}^{-1}$, $x_{\text{BT}} = 0.058$, $x_{\text{DMBT}} = 0.046$, $J/k(\text{BT}) = -765(9) \text{ K}$ (-532 cm^{-1}) and $J/k(\text{DMBT}) = -587(9) \text{ K}$ (-408 cm^{-1}).

3. Conclusions

We have shown here that the tetrathiafulvalenyl diphosphine platinum bis(thiolate) complexes $(\mathbf{P2})\text{Pt}(\text{BT})_2$ and $(\mathbf{P2})\text{Pt}(\text{DMBT})_2$ exhibit a low potential irreversible oxidation wave not observed in the $(\mathbf{P2})\text{PtCl}_2$ complex. Based on the behavior of analogous (dppe)

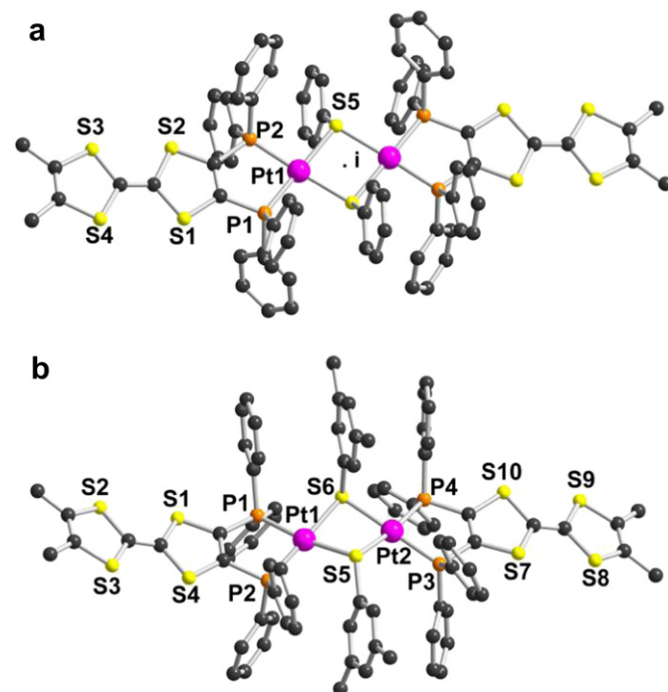


Fig. 4. Molecular structures of (a) $[(\mathbf{P2})\text{Pt}(\mu\text{-BT})_2\text{Pt}(\mathbf{P2})]^{2+}$ and (b) $[(\mathbf{P2})\text{Pt}(\mu\text{-DMBT})_2\text{Pt}(\mathbf{P2})]^{2+}$ in the form of their TCNQF_4^- salts.

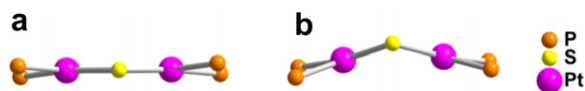


Fig. 5. Geometries of $\{Pt_2Pt(\mu-S)_2PtPt_2\}$ core observed in (a) $[(P_2)Pt(\mu-BT)_2Pt(P_2)]^{2+}$ (planar) and (b) $[(P_2)Pt(\mu-DMBT)_2Pt(P_2)]^{2+}$ (bent).

Pt(BT)₂ and (dppe)Pt(DMBT)₂ complexes lacking the TFF redox core, it was tentatively associated to thiolate oxidation. This was further confirmed by the TCNQF₄ oxidation of the two complexes, which affords dicationic $[(P_2)Pt(\mu-SAr)_2Pt(P_2)]^{2+}$ species. Their formations are associated with loss (and potential oxidation) of one thiolate ligand, as tentatively illustrated in Scheme 5, with the reduced TCNQF₄ radical anion precipitating as radical anion with the dimerized dicationic species, $[(P_2)Pt(\mu-SAr)_2Pt(P_2)]^{2+}$.

It should be also emphasized here that this oxidative dimerization mechanism for the formation of the $\{Pt_2(\mu-SAr)_2\}$ bimetallic square motif complements the other previously described methods, which involved (i) the alkylation of a pre-formed $\{Pt_2S_2\}$ motif [15], (ii) the *in situ* combination (metathesis) of (P–P)Pt and bridging thiolate ligand [25], (iii) the nucleophilic displacement (metathesis) of the triflate leaving group by a pre-formed (P–P)Pt(SR)₂ complex [24], and (iv) the ring-opening of the thiaplatina-cycle [30]. It provides a potential better approach to the synthesis of such bimetallic complexes particularly adapted to electron-rich thiolate ligands, but whose promise has yet to be demonstrated with other diphosphines than **P2**.

The crystallographic determinations of the two bimetallic compounds, $[(P_2)Pt(\mu-BT)_2Pt(P_2)]^{2+}$ and $[(P_2)Pt(\mu-DMBT)_2Pt(P_2)]^{2+}$, give also two other examples of structural flexibility in such bimetallic systems incorporating the $\{Pt_2S_2\}$ square motif with bridging RS[–] and/or S^{2–} ligands [15,16].

4. Experimental

4.1. General procedures

First grade organic solvents were purchased and used without further purification. They were degassed by bubbling Ar prior to use. All reactions and recrystallizations involving Pt(II) complexes were carried out under protection from light and air. The starting Pt complex **(P2)**PtCl₂ was prepared as previously described [9g] from **P2** [9a]. The melting points were determined using a Stuart SMP3 (Barloworld Scientific Ltd.). The MALDI-TOF mass spectra were measured with a Voyager-DE™ STR Biospectrometry Workstation (Applied Biosystems Inc.). The infrared spectra were recorded by the KBr pellet method on a Perkin Elmer Spectrum 100 in the range of 4000–400 cm^{–1}. The ¹H/³¹P NMR measurements were performed at room temperature using an Avance 500 (Bruker, 500 MHz) with the samples dissolved in CDCl₃. The positive chemical shifts are reported downfield from the external standards, viz. 85% H₃PO₄ for the ³¹P{¹H} resonances. The UV/vis spectra were obtained on an HP 8452A diode array spectrophotometer in CH₂Cl₂. The cyclic voltammetry (CV) measurements were carried out at

Table 3
Selected bond distances (Å) and angles (°) in $[(P_2)Pt(\mu-BT)_2Pt(P_2)](TCNQF_4)_2$.

Distance (Å)		Angle (°)	
Pt(1)–P(1)	2.2766(9)	P(1)–Pt(1)–P(2)	87.19(3)
Pt(1)–P(2)	2.2548(10)	P(2)–Pt(1)–S(5) ^j	94.09(3)
Pt(1)–S(5)	2.3784(9)	S(5)–Pt(1)–S(5)	81.64(3)
Pt(1)–S(5) ^j	2.3879(9)	P(1)–Pt(1)–S(5)	97.39(3)
Pt(1)···Pt(1) ^j	3.607(6)	P(2)–Pt(1)–S(5) ^j	94.09(3)
S(5)···S(5) ^j	3.116(8)	Pt(1)–S(5)–Pt(1) ⁱ	98.36(3)

Symmetry code: ⁱ –x, –y, –z.

Table 4
Selected bond distances (Å) and angles (°) in $[(P_2)Pt(\mu-DMBT)_2Pt(P_2)](TCNQF_4)_2$.

Distance (Å)		Angle (°)	
Pt(1)–P(1)	2.253(3)	P(1)–Pt(1)–P(2)	86.11(10)
Pt(1)–P(2)	2.264(3)	P(2)–Pt(1)–S(5)	100.01(9)
Pt(1)–S(5)	2.362(3)	P(1)–Pt(1)–S(6)	92.81(10)
Pt(1)–S(6)	2.374(3)	S(5)–Pt(1)–S(6)	81.22(9)
Pt(2)–P(3)	2.257(3)	P(3)–Pt(2)–P(4)	87.83(10)
Pt(2)–P(4)	2.263(3)	P(3)–Pt(2)–S(5)	98.28(10)
Pt(2)–S(5)	2.372(3)	P(4)–Pt(2)–S(6)	92.91(9)
Pt(2)–S(6)	2.375(3)	S(5)–Pt(2)–S(6)	80.99(9)
Pt(1)···Pt(2)	3.4562(7)	Pt(1)–S(5)–Pt(2)	93.79(9)
S(5)···S(6)	3.082(4)	Pt(1)–S(6)–Pt(2)	93.41(9)

room temperature with a CHI 620A Electrochemical Analyzer (CHI Instrument Inc.) in 3 mL of CH₂Cl₂ solution containing 1 mM of the sample, using 0.1 M *n*-Bu₄N⁺PF₆[–] as the supporting electrolyte, Ag/AgCl as a reference electrode, a Pt button working electrode, a Pt wire as the counter electrode and with a scan rate of 50 mV s^{–1}. All redox potentials were referenced against the Fc⁺/Fc redox couple (*E*_{1/2} = 0.565 V). The magnetic susceptibility measurements were obtained with the use of a Quantum Design SQUID magnetometer MPMS-XL. This magnetometer works between 1.8 and 400 K for DC applied fields ranging from –5 to 5 T. The measurements were performed at 5 kG on polycrystalline TCNQF₄ salts of the BT (3.2 mg) and DMBT (6.3 mg). The magnetic data were corrected for the sample holder and the diamagnetic contributions.

4.2. Preparation of **(P2)**Pt(SAr)₂ complexes

A CH₂Cl₂ solution (25 mL) of **(P2)**PtCl₂ (0.2 mmol, 173 mg), triethylamine (0.8 mmol, 81 mg) and aryl thiol (0.4 mmol, 55 mg) for 3,5-dimethylbenzenethiol (DMBT-H) 44 mg for benzenethiol (BT-H) was stirred for 24 h at room temperature under an argon atmosphere. The red-orange solution was evaporated and the solid residue was purified by column chromatography (SiO₂, CH₂Cl₂). The red-orange products were recrystallized from CH₂Cl₂/MeOH.

(P2)Pt(BT)₂. Yield: 69% (140 mg); m.p. >275 °C (decomp.); ¹H NMR (300 MHz, CDCl₃, TMS): δ = 7.76 (m, 8H, Ph), 7.47 (m, 12H, Ph), 7.02 (m, 4H, CH in BT), 6.70 (m, 6H, CH in BT), 1.87 ppm (s, 6H, CH₃ in

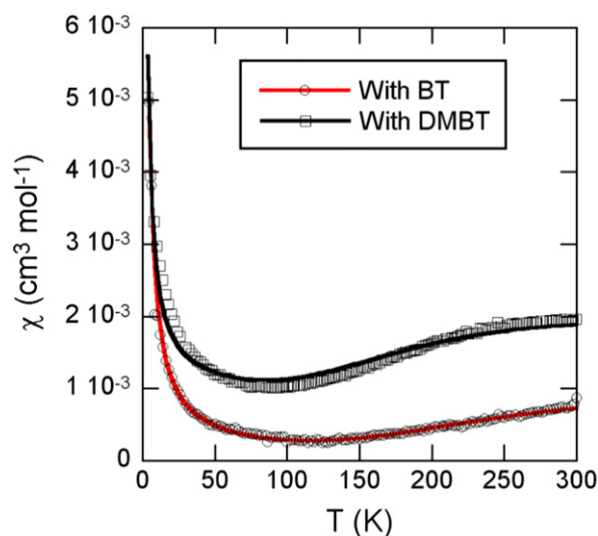


Fig. 6. Temperature dependence of the magnetic susceptibility for $[(P_2)Pt(\mu-BT)_2Pt(P_2)]^{2+}(TCNQF_4)_2$ and $[(P_2)Pt(\mu-DMBT)_2Pt(P_2)]^{2+}(TCNQF_4)_2$. Solid lines are fits to the singlet-triplet model (see text).

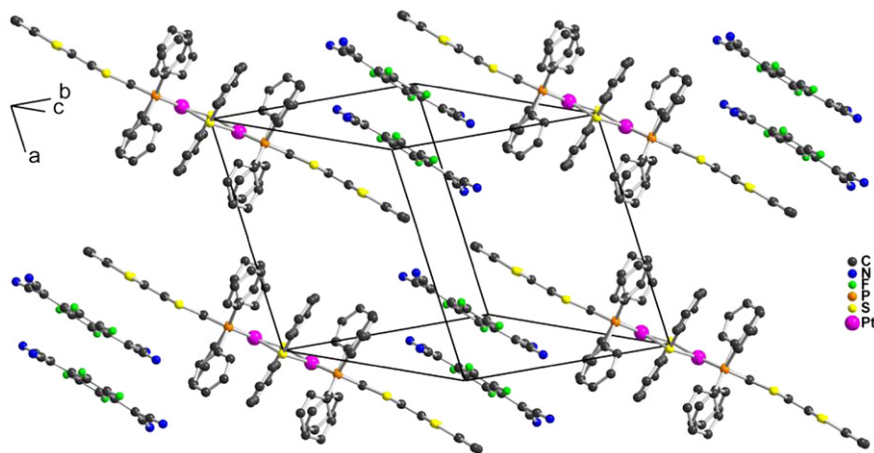


Fig. 7. View of the solid state organization within one layer in $[(\mathbf{P2})\text{Pt}(\mu\text{-BT})_2\text{Pt}(\mathbf{P2})][(\text{TCNQF}_4)_2]$, with $[(\text{TCNQF}_4)_2]^{2-}$ dimers sandwiched between the TTF moieties. Solvent molecules and hydrogen atoms were omitted for clarity.

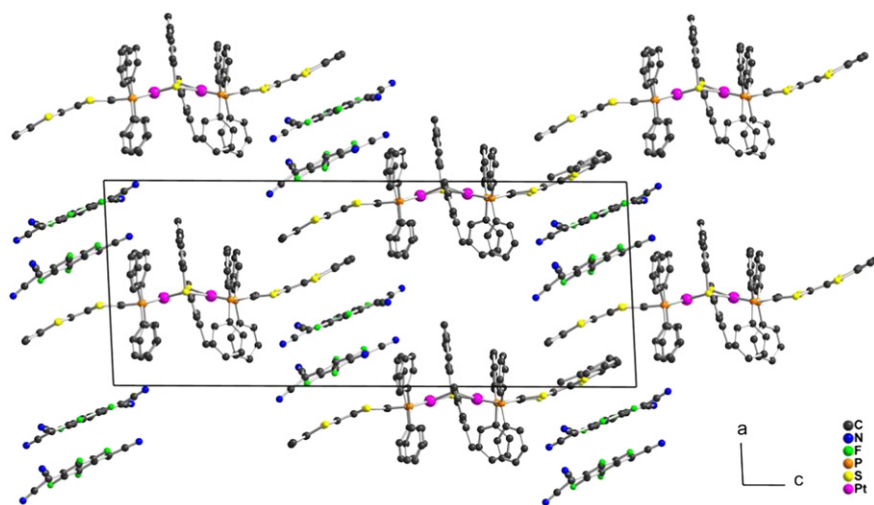


Fig. 8. View of the solid state organization within one layer in $[(\mathbf{P2})\text{Pt}(\mu\text{-DMBT})_2\text{Pt}(\mathbf{P2})][(\text{TCNQF}_4)_2]$, with $[(\text{TCNQF}_4)_2]^{2-}$ dimers sandwiched between the TTF moieties. Solvent molecules and hydrogen atoms were omitted for clarity.

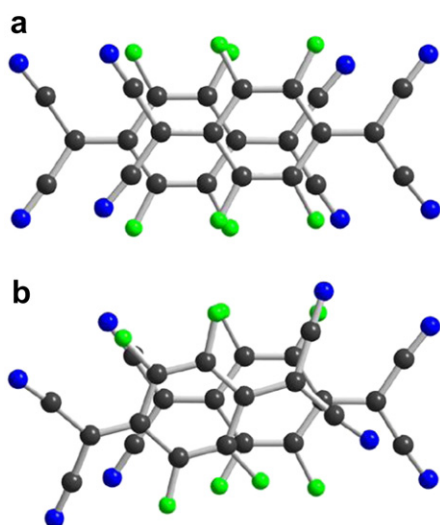
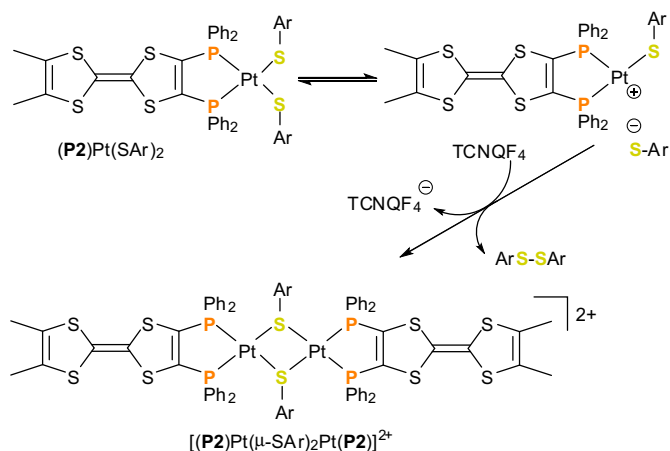


Fig. 9. Overlap modes of TCNQF_4 observed in $[(\mathbf{P2})\text{Pt}(\mu\text{-SAr})_2\text{Pt}(\mathbf{P2})]^{2+}[(\text{TCNQF}_4)_2]^{2-}$ where SAr is (a) BT and (b) DMBT.

TTF); ^{31}P NMR (121 MHz, CDCl_3 , 85% H_3PO_4): $\delta = 31.99$ ppm ($J_{\text{Pt-P}} = 2862$ Hz); FT-IR (KBr): 3058 (Ar C–H), 2989, 2913 (– CH_3), 1577, 1480, 1469, 1434 (Ar C=C), 1101, 1085 (P–Ph), 1023, 1008, 998 (Ar C–H ip def), 882 (asym S–C–S), 731, 686 (Ar C–H oop def) $548, 520, 484\text{ cm}^{-1}$ (Ar ring oop def); UV/vis (CH_2Cl_2): $\lambda_{\text{max}} = 232$ (s), 276 (m), 340 (sh), 420 nm (w); MALDI-TOFMS: m/z (%) 1012.8970 (1) $[\text{M}^+]$; 904.9208 (100) $[\text{M}^+ - \text{SC}_6\text{H}_5]$. EA calcd for $\text{C}_{44}\text{H}_{36}\text{P}_2\text{PtS}_6$ (MW: 1013.14 g/mol): C 52.12; H 3.58%. Found: C 51.92; H 3.62%.

$(\mathbf{P2})\text{Pt}(\text{DMBT})_2$. Yield: 62% (133 mg); m.p. 256–257 °C; ^1H NMR (500 MHz, CDCl_3 , TMS): $\delta = 7.72$ (m, 8H, Ph), 7.46 (t, 4H, Ph), 7.39 (t, 8H, Ph), 6.64 (s, 4H, CH in DMBT), 6.32 (s, 2H, CH in DMBT), 1.88 (s, 12H, CH_3 in DMBT), 1.86 ppm (s, 6H, CH_3 in TTF); ^{31}P NMR (202 MHz, CDCl_3 , 85% H_3PO_4): $\delta = 32.12$ ppm ($J_{\text{Pt-P}} = 2888$ Hz); FT-IR (KBr): 3049, 3020 (Ar C–H), 2912, 2853 (– CH_3), 1594, 1574, 1480, 1434 (Ar C=C), 1099 (P–Ph), 1027, 1008, 999 (Ar C–H ip def), 839 (asym S–C–S), 744, 689 (Ar C–H oop def), 546, 519, 480 cm^{-1} (Ar ring oop def); UV/vis (CH_2Cl_2): $\lambda_{\text{max}} = 232$ (s), 276 (m), 340 (sh), 420 nm (w); MALDI-TOF MS: m/z (%) 1068.9532 (1) $[\text{M}^+]$, 932.9751 (100) $[\text{M}^+ - \text{SC}_6\text{H}_3\text{Me}_2]$. EA calcd for $\text{C}_{48}\text{H}_{44}\text{P}_2\text{PtS}_6$ (MW: 1069.20 g/mol): C 53.87; H 4.15%. Found: C 53.69; H 4.20%.



Scheme 5. The proposed dimerization process to the $[(\mathbf{P2})\text{Pt}(\mu\text{-SAr})_2\text{Pt}(\mathbf{P2})]^{2+}$ dication.

4.3. Preparation of $(dppe)\text{Pt}(\text{SAr})_2$ complexes

An acetone solution (5 mL) of $\text{Pb}(\text{SAr})_2$ [19] (0.1 mmol, $\text{SAr} = \text{DMBT}$ (48 mg) and BT (43 mg)) was added to an acetone suspension (5 mL) of $(dppe)\text{PtCl}_2$ (0.1 mmol, 66 mg) with stirring for 24 h at room temperature. The PbCl_2 precipitate was separated by filtration and the purified product was recrystallized from acetone/pentane.

$(dppe)\text{Pt}(\text{BT})_2$. Yield: 15% (12.0 mg); m.p. >188 °C (decomp); ^1H NMR (300 MHz, CDCl_3 , TMS): $\delta = 7.65$ (m, 8H, Ph), 7.36 (m, 12H, Ph), 7.05 (m, 4H, CH in BT), 6.61 (m, 6H, CH in BT), 2.18 ppm (s, 4H, $\text{PCH}_2\text{CH}_2\text{P}$); ^{31}P NMR (121 MHz, CDCl_3 , 85% H_3PO_4): $\delta = 45.78$ ppm ($J_{\text{Pt-P}} = 2880$ Hz); FT-IR (KBr): 3051 (Ar C–H), 1577, 1484, 1471, 1435 (Ar C=C), 1102, 1085 (P–Ph), 1025, 998 (Ar C–H ip def), 880 (asym S–C–S), 749, 735, 689 (Ar C–H oop def) 530, 486 cm^{-1} (Ar ring oop def); UV/vis (CH_2Cl_2): $\lambda_{\text{max}} = 232$ (s), 262 (m), 360 nm (w). EA calcd for $\text{C}_{38}\text{H}_{34}\text{P}_2\text{PtS}_2$ (MW: 811.24 g/mol): C 56.22; H,

4.22. Found: C, 55.27; H, 4.20%. Inclusion of one water molecule gives calculated values for $\text{C}_{38}\text{H}_{34}\text{P}_2\text{PtS}_2 \cdot \text{H}_2\text{O}$: C, 55.00; H, 4.37, which is in good accordance with the experimental values.

$(dppe)\text{Pt}(\text{DMBT})_2$. Yield: 15% (12.6 mg); m.p. >160 °C (decomp); ^1H NMR (300 MHz, CDCl_3 , TMS): $\delta = 7.66$ (m, 8H, Ph), 7.33 (m, 12H, Ph), 6.71 (s, 4H, CH in DMBT), 6.31 (s, 2H, CH in DMBT), 2.21 (s, 4H, $\text{PCH}_2\text{CH}_2\text{P}$), 1.86 ppm (s, 12H, CH_3 in DMBT); ^{31}P NMR (121 MHz, CDCl_3 , 85% H_3PO_4): $\delta = 46.26$ ppm ($J_{\text{Pt-P}} = 2951$ Hz); FT-IR (KBr): 3051, 3021 (Ar C–H), 2914, 2856 ($-\text{CH}_3$), 1595, 1575, 1464, 1434 (Ar C=C), 1104 (P–Ph), 1028, 998 (Ar C–H ip def), 840 (asym S–C–S), 747, 75, 689 (Ar C–H oop def), 532, 486 cm^{-1} (Ar ring oop def); UV/vis (CH_2Cl_2): $\lambda_{\text{max}} = 230$ (s), 260 nm (sh). EA calcd for $\text{C}_{42}\text{H}_{42}\text{P}_2\text{PtS}_2$ (MW: 867.96 g/mol): C 58.12; H 4.88%. Found: C 57.95; H 4.75%.

4.4. Preparation of TCNQF_4 salts

$[(\mathbf{P2})\text{Pt}(\mu\text{-BT})_2\text{Pt}(\mathbf{P2})](\text{TCNQF}_4)_2 \cdot (\text{PhCl})_4$. To a chlorobenzene solution (1 mL) of $(\mathbf{P2})\text{Pt}(\text{BT})_2$ (0.01 mmol, 10 mg) was added a chlorobenzene solution (1 mL) of TCNQF_4 (0.01 mmol, 2.8 mg). The dark green solution was heated at 70 °C for 40 min. Some black crystals began to form, as the reaction solution was stored in a freezer. The product was filtered off, washed with cold chlorobenzene and dried under vacuum.

FT-IR (KBr): 2192, 2170 cm^{-1} ($\text{C}\equiv\text{N}$). EA calcd for $\text{C}_{124}\text{H}_{82}\text{Cl}_4\text{F}_8\text{N}_8\text{P}_4\text{Pt}_2\text{S}_{10}$ (MW: 2812.52 g/mol): C 52.92; H 2.94; N 3.99; Found: C 52.68; H 3.10; N 4.74.

$[(\mathbf{P2})\text{Pt}(\mu\text{-DMBT})_2\text{Pt}(\mathbf{P2})](\text{TCNQF}_4)_2 \cdot (\text{PhCH}_3)(\text{CHCl}_3)_3$. To a toluene solution (0.8 mL) of $(\mathbf{P2})\text{Pt}(\text{DMBT})_2$ (0.01 mmol, 11 mg) was added a CHCl_3 (1.3 mL) and toluene solution (0.2 mL) of TCNQF_4 (0.01 mmol, 3 mg). The dark green solution was heated at 55 °C for 40 min. Some black crystals began to form as the reaction solution cooled down to room temperature and the solution was then stored in a freezer. The product was filtered off, washed with cold chlorobenzene and dried under vacuum.

FT-IR (KBr): 2192, 2170 cm^{-1} ($\text{C}\equiv\text{N}$). EA calcd for $\text{C}_{114}\text{H}_{81}\text{Cl}_9\text{F}_8\text{N}_8\text{P}_4\text{Pt}_2\text{S}_{10}$ (MW: 2866.50 g/mol): C 47.73; H 2.85; N 3.91. Found: C 48.09; H 2.53; N 4.03.

Table 5

Crystal data and structure refinement parameters for platinum(II) complexes.

	$(\mathbf{P2})\text{Pt}(\text{DMBT})_2$	$(\mathbf{P2})\text{Pt}(\text{BT})_2$	$[(\mathbf{P2})\text{Pt}(\mu\text{-BT})_2\text{Pt}(\mathbf{P2})](\text{TCNQF}_4)_2 \cdot 4\text{PhCl}$	$[(\mathbf{P2})\text{Pt}(\mu\text{-DMBT})_2\text{Pt}(\mathbf{P2})](\text{TCNQF}_4)_2 \cdot \text{MePh} \cdot 3\text{CHCl}_3$
Formula	$\text{C}_{48}\text{H}_{44}\text{P}_2\text{PtS}_6$	$\text{C}_{44}\text{H}_{36}\text{P}_2\text{PtS}_6$	$\text{C}_{124}\text{H}_{82}\text{Cl}_4\text{F}_8\text{N}_8\text{P}_4\text{Pt}_2\text{S}_{10}$	$\text{C}_{114}\text{H}_{81}\text{Cl}_9\text{F}_8\text{N}_8\text{P}_4\text{Pt}_2\text{S}_{10}$
Formula weight	1070.22	1014.12	2812.52	2868.58
Crystal system	Monoclinic	Monoclinic	Triclinic	Monoclinic
Space group	$P2_1/c$	$P2_1/n$	$P-1$	$P2_1/n$
<i>a</i> (Å)	9.0616(5)	16.0528(6)	14.0911(11)	15.0588(11)
<i>b</i> (Å)	23.8498(15)	15.9253(6)	14.6513(10)	20.2005(13)
<i>c</i> (Å)	20.7935(14)	17.3584(7)	14.7880(11)	38.277(3)
α (°)	90.00	90.00	80.652(4)	90.00
β (°)	94.005(2)	110.567(2)	72.806(4)	92.896(2)
γ (°)	90.00	90.00	82.403(4)	90.00
Volume (Å ³)	4482.9(5)	4154.8(3)	2866.0(4)	11628.8(14)
<i>Z</i>	4	4	1	4
<i>D</i> _{calc} (Mg/m ³)	1.586	1.621	1.630	1.638
μ (mm ⁻¹)	3.515	3.788	2.837	2.910
<i>F</i> (000)	2144	2016	1398	5688
Cryst. size (mm ³)	0.5 × 0.3 × 0.2	0.3 × 0.2 × 0.1	0.3 × 0.1 × 0.05	0.1 × 0.06 × 0.01
θ range (°)	1.30–27.47	1.49–27.46	2.42–27.55	1.07–27.54
Index ranges	–11 ≤ <i>h</i> ≤ 7 –30 ≤ <i>k</i> ≤ 30 –26 ≤ <i>l</i> ≤ 26	–16 ≤ <i>h</i> ≤ 20 –20 ≤ <i>k</i> ≤ 20 –22 ≤ <i>l</i> ≤ 18	–18 ≤ <i>h</i> ≤ 18 –18 ≤ <i>k</i> ≤ 18 –19 ≤ <i>l</i> ≤ 17	–19 ≤ <i>h</i> ≤ 19 –18 ≤ <i>k</i> ≤ 26 –49 ≤ <i>l</i> ≤ 49
<i>T</i> _{min} , <i>T</i> _{max}	0.293, 0.495	0.419, 0.685	0.719, 0.868	0.811, 0.971
Data/restr./param.	10,245/0/520	9496/0/480	12,654/68/787	26,785/0/1392
GOF	1.084	1.128	1.188	1.074
<i>wR</i> (<i>F</i> ²) [all data]	0.1068	0.0956	0.0982	0.1613
<i>R</i> (<i>F</i>) [<i>I</i> > 2σ(<i>I</i>)]	0.0311	0.0316	0.0301	0.0716
Res. dens. (e/Å ³)	–1.06, 1.01	–1.74, 0.79	–1.84, 2.93	–2.14, 2.44

4.5. X-ray crystallography

The experimental data and refinement results are given in Table 5. The data were collected on an APEX II Bruker AXS diffractometer with Mo-K α radiation ($\lambda = 0.71073$ Å) at 100 K. The SADABS absorption correction was applied. The structures were solved by direct methods (SHELXS97 [31] or SIR) and refined (SHELXL-97) [31] by full-matrix least-squares methods as implemented in the WinGX software package [32]. Hydrogen atoms were introduced at the calculated positions (riding model) included in the structure factor calculation but not refined. [(P2)Pt(μ -BT)₂Pt(P2)](TCNQF₄)₂ crystallizes with four PhCl solvent molecules, one located in general position and two disordered on inversion centers. Restraints (FREE instructions) were only used to disconnect the carbon atoms of the two disordered molecules in order to allow the generation of H atoms by the HFIX instruction. [(P2)Pt(μ -DMBT)₂Pt(P2)](TCNQF₄)₂ crystallizes with one toluene and three chloroform molecules, all in general position. One carbon atom C(2) of the TTF core, bonded to P(2) could only be refined isotropically.

Acknowledgments

This French-Korean collaborative work was supported by the bilateral STAR program under the reference numbers 19036SM and 12974RC, as well as by the CNRS (France) and the University Rennes 1 through the GDRI program “Functional Material for Organic Optics, Electronics, and Devices” (FUN MOOD). Work at Seoul Women’s University was supported by Basic Science Research Program through the National Research Foundation of Korea (NRF) funded by the Ministry of Education, Science and Technology (NRF2010-0011478). We thank CDIFX (Rennes) for access to X-ray diffractometers for X-ray data collections.

Appendix A. Supplementary material

CCDC 826353–826356 contains the supplementary crystallographic data for (P2)Pt(BT)₂, (P2)Pt(DMBT)₂, [(P2)Pt(μ -DMBT)₂Pt(P2)](TCNQF₄)₂·MePh·3CHCl₃ and [(P2)Pt(μ -DMBT)₂Pt(P2)](TCNQF₄)₂·4PhCl, respectively. These data can be obtained free of charge at www.ccdc.cam.ac.uk/conts/retrieving.html or from the Cambridge Crystallographic Data Centre, 12 Union Road, Cambridge CB2 1EZ, UK [fax: +44 1223/336 033. E-mail: deposit@ccdc.cam.ac.uk].

References

- [1] V.K. Jain, L. Jain, *Coord. Chem. Rev.* 249 (2005) 3075–3197.
- [2] (a) K.S. Shin, K.I. Son, J.I. Kim, C.S. Hong, M. Suh, D.Y. Noh, *Dalton Trans.* (2009) 1767–1775; (b) K.S. Shin, D.Y. Noh, *Bull. Korean Chem. Soc.* 29 (2008) 2533–2536; (c) D.Y. Noh, K.S. Shin, K.I. Son, *Bull. Korean Chem. Soc.* 28 (2007) 343–346; (d) K.S. Shin, D.Y. Noh, *Bull. Korean Chem. Soc.* 25 (2004) 130–132.
- [3] P.C.A. Bruijninx, P.J. Sadler, *Curr. Opin. Chem. Biol.* 12 (2008) 197–206.
- [4] (a) S.W. Chien, T.S. Andy Hor, in: P. Štěpnička (Ed.), *Ferrocenes: Ligands, Materials and Biomolecules*, Wiley, Chichester, 2008, pp. 33–116; (b) B. Cornils, W.A. Herrmann, *Applied Homogeneous Catalysis with Organometallic Compounds*, Wiley-VCH, Weinheim, 2002.
- [5] (a) S.D. Cummings, R. Eisenberg, in: E.I. Stiefel (Ed.), *Progress in Inorganic Chemistry*, vol. 52, John Wiley, NJ, 2004, pp. 315–367; (b) K.A. Van Houten, R.S. Pilato, in: E.I. Stiefel (Ed.), *Progress in Inorganic Chemistry*, vol. 52, John Wiley, NJ, 2004, pp. 369–397.
- [6] R. Kato, *Chem. Rev.* 104 (2004) 5319–5346.
- [7] (a) S.K. Lee, D.Y. Noh, *Inorg. Chem. Commun.* 13 (2010) 183–186; (b) K.S. Shin, Y.K. Han, D.Y. Noh, *Bull. Korean Chem. Soc.* 24 (2003) 235–238; (c) D.Y. Noh, E.M. Seo, H.J. Lee, H.Y. Jang, M.G. Choi, Y.H. Kim, J. Hong, *Polyhedron* 20 (2001) 1939–1945.
- [8] W.S. Han, Y.J. Kim, S.W. Lee, *Bull. Korean Chem. Soc.* 24 (2003) 60–64.
- [9] (a) M. Fourmigué, P. Batail, *Bull. Soc. Chim. Fr.* 129 (1992) 29–36; (b) M. Fourmigué, C.E. Uzelmeier, K. Boubekour, S.L. Bartley, K.R. Dunbar, *J. Organomet. Chem.* 529 (1997) 343–350; (c) N. Avarvari, D. Martin, M. Fourmigué, *J. Organomet. Chem.* 643/644 (2002) 292–300; (d) C.E. Uzelmeier, S.L. Bartley, M. Fourmigué, R. Rogers, G. Grandinetti, K.R. Dunbar, *Inorg. Chem.* 37 (1998) 6706–6713; (e) C.E. Uzelmeier, B.W. Smucker, E.W. Reinheimer, M. Shatruck, A.W. O’Neal, M. Fourmigué, K.R. Dunbar, *Dalton Trans.* (2006) 5259–5268; (f) B.W. Smucker, K.R. Dunbar, *Dalton Trans.* (2000) 1309–1315; (g) T. Devic, P. Batail, M. Fourmigué, N. Avarvari, *Inorg. Chem.* 43 (2004) 3136–3141; (h) C. Gouverd, F. Biaso, L. Cataldo, T. Berclaz, M. Geoffroy, E. Levillain, N.M. Fourmigué, F.X. Sauvage, C. Wartelle, *Phys. Chem. Chem. Phys.* 7 (2005) 85–93.
- [10] S.K. Lee, K.S. Shin, D.Y. Noh, O. Jeannin, F. Barrière, J.F. Bergamini, M. Fourmigué, *Chem. Asian J.* 5 (2010) 169–176.
- [11] K.S. Shin, Y.J. Jung, S.K. Lee, M. Fourmigué, F. Barrière, J.F. Bergamini, D.Y. Noh, *Dalton Trans.* (2008) 5869–5871.
- [12] R. Vicente, J. Ribas, X. Solans, M. Font-Altaba, A. Mari, P. De Loth, P. Cassoux, *Inorg. Chim. Acta* 132 (1987) 229–236.
- [13] A. Garcés-Rodríguez, D. Morales-Morales, S. Hernández-Ortega, *Acta Crystallogr. Sect. E63* (2007) m479–m481.
- [14] L.L. Maisela, A.N. Crouch, J. Darkwa, I.A. Guzei, *Polyhedron* 20 (2001) 3189–3200.
- [15] (a) S.W.A. Fong, T.S.A. Hor, *J. Chem. Soc., Dalton Trans.* (1999) 639–651; (b) S.H. Chong, L.L. Koh, W. Henderson, T.S.A. Hor, *Chem. Asian J.* 1 (2006) 264–272; (c) S.H. Chong, D.J. Young, T.S.A. Hor, *Chem. Asian J.* 2 (2007) 1356–1362; (d) S.H. Chong, W. Henderson, T.S.A. Hor, *Dalton Trans.* (2007) 4008–4016; (e) J. Li, F. Li, L.L. Koh, T.S.A. Hor, *Dalton Trans.* 39 (2010) 2441–2448.
- [16] (a) P. González-Duarte, A. Lledós, R. Mas-Ballesté, *Eur. J. Inorg. Chem.* (2004) 3585–3599; (b) R. Mas-Ballesté, G. Aullón, P.A. Champkin, W. Clegg, C. Mégrét, P. González-Duarte, A. Lledós, *Chem. Eur. J.* 9 (2003) 5023–5035; (c) M. Capdevila, W. Clegg, P. González-Duarte, A. Jarid, A. Lledós, *Inorg. Chem.* 35 (1996) 490–497; (d) M. Capdevila, W. Clegg, P. González-Duarte, B. Harris, I. Mira, J. Sola, I.C. Taylor, *J. Chem. Soc., Dalton Trans.* (1992) 2817–2826.
- [17] C. Eaborn, K.J. Odell, A. Pidcock, *J. Organomet. Chem.* 170 (1979) 105–115.
- [18] R.D. Lai, A. Shaver, *Inorg. Chem.* 20 (1981) 477–480.
- [19] (a) S.E. Appleton, G.G. Briand, A. Decken, A.S. Smith, *Dalton Trans.* (2004) 3515–3520; (b) M.E. Peach, *Can. J. Chem.* 46 (1968) 2699–2706.
- [20] R.C. Wheland, J.L. Gilson, *J. Am. Chem. Soc.* 98 (1976) 3916–3925.
- [21] For correlation of redox potential with chemical oxidation power, see also: N.G. Connelly, W.E. Geiger *Chem. Rev.* 96 (1996) 877–910.
- [22] G.W. Wei, Z.Y. Huang, M.C. Hong, H.Q. Liu, Jiégou Huaxue (Chin. J. Struct. Chem.) 10 (1991) 159–160 (CCDC KIXGUT), CA 115:244479.
- [23] R.H. Vaz, R.M. Silva, J.H. Reibenspies, O.A. Serra, *J. Braz. Chem. Soc.* 13 (2002) 82–87.
- [24] G. Rivera, S. Bernes, H. Torrens, *Polyhedron* 26 (2007) 4276–4286.
- [25] C. Mendoza, J. Benet-Buchholz, M.A. Pericás, R. Vilar, *Dalton Trans.* (2009) 2974–2985.
- [26] (a) C. Wartelle, R. Viruela, P.M. Viruela, F.X. Sauvage, M. Sallé, E. Orti, E. Levillain, F. Le Derf, *Phys. Chem. Chem. Phys.* 5 (2003) 4672–4679; (b) P.R. Ashton, V. Balzani, J. Becker, A. Credi, M.C.T. Fyfe, G. Matternsteig, S. Menzer, M.B. Nielsen, F.M. Raymo, J.F. Stoddart, M. Venturi, D.J. Williams, *J. Am. Chem. Soc.* 121 (1999) 3951–3957.
- [27] N. Avarvari, M. Fourmigué, *Chem. Commun.* (2004) 1300–1301.
- [28] T. Sugimoto, K. Ueda, M. Tsujii, H. Fujita, N. Hosoito, N. Kanehisa, Y. Shibamoto, Y. Kai, *Chem. Phys. Lett.* 249 (1996) 304–308.
- [29] (a) J.S. Miller, J.H. Zhang, W.M. Reiff, *Inorg. Chem.* 26 (1987) 600–608; (b) D.A. Dixon, J.C. Calabrese, J.S. Miller, *J. Phys. Chem.* 93 (1989) 2284–2291.
- [30] J.J. Garcia, A. Arevalo, V. Montiel, F. Del Rio, B. Quiroz, H. Adams, P. Maitlis, *Organometallics* 16 (1997) 3216–3220.
- [31] G.M. Sheldrick, *SHELX97-Programs for Crystal Structure Analysis* (Release 97-2) (1998).
- [32] L.J. Farrugia, *J. Appl. Cryst.* 32 (1999) 837–838.